frontiers | Frontiers in Marine Science

TYPE Original Research
PUBLISHED 29 January 2024
DOI 10.3389/fmars.2024.1338832

OPEN ACCESS

EDITED BY
Khan M. G. Mostofa,
Tianjin University, China

REVIEWED BY
Amit Kumar,
Nanjing University of Information Science and Technology, China
Maribel I. García-Ibáñez,
Spanish Institute of Oceanography (IEO), Spain
Alban Kuriqi,
University of Lisbon, Portugal

*CORRESPONDENCE
Tae-Wook Kim
kimtwk@korea.ac.kr

RECEIVED 15 November 2023
ACCEPTED 12 January 2024
PUBLISHED 29 January 2024

CITATION
Ko YH and Kim T-W (2024) Assessment of the potential effect of thermal effluents on CO_2 absorption in coastal waters.
Front. Mar. Sci. 11:1338832.
doi: 10.3389/fmars.2024.1338832

Assessment of the potential effect of thermal effluents on CO_2 absorption in coastal waters

Young Ho Ko[1] and Tae-Wook Kim[1,2]*

[1]OJEong Resilience Institute, Korea University, Seoul, Republic of Korea, [2]Division of Environmental Science and Ecological Engineering, Korea University, Seoul, Republic of Korea

In recent decades, the cooling water discharge (CWD) from thermoelectric power plants into coastal waters has increased. The higher temperatures at the discharge outlets can elevate the seawater partial pressure of carbon dioxide (pCO_2), potentially resulting in increased carbon dioxide (CO_2) emissions or reduced CO_2 absorption. Using a comprehensive global power plant database, we evaluated the impact of CWD on surface water CO_2. Our assessment suggests that CWD from coastal power plants has the potential to contribute to a decline in oceanic CO_2 uptake by 0.09–0.69 Tg C yr^{-1} (equivalent to 0.3–2.5 Tg CO_2 yr^{-1}). This estimation considered solely the influence of air–sea CO_2 exchange, excluding the impact of air–sea heat exchange following cooling water discharge. Therefore, our estimate of 0.09–0.69 Tg C yr^{-1} is likely an upper theoretical limit. While our estimate appears minor in relation to global estimates of the oceanic CO_2 flux, this impact of CWD should be addressed on a national scale. For precise quantification of the impact of CWD on local air–sea CO_2 flux, accurate information on environmental factors such as wind speeds, mixed layer depth, and background carbonate chemistry is essential.

KEYWORDS

power plant, thermal discharge, coastal ocean, pCO2, air-sea CO2 flux

1 Introduction

In line with the goal of the Paris Agreement objective to limit the increase in the global temperature to 1.5–2.0°C above pre-industrial levels (Hoegh-Guldberg et al., 2019), the sequestration of anthropogenic CO_2 in the ocean, accounting for 26% of emissions over the last decade, is crucial for climate change mitigation (Friedlingstein et al., 2022). The rise in the global ocean temperature attributed to anthropogenic CO_2 production has reduced oceanic CO_2 uptake through air–sea gas exchange and strengthened water stratification,

Abbreviations: α, CO_2 solubility in seawater; CO_2, Carbon dioxide; CWD, Cooling water discharge; DIC, Total dissolved inorganic carbon; FCO_2, Air–sea CO_2 flux; *k*, CO_2 gas transfer velocity; pCO_2, Partial pressure of CO_2 in seawater; Sc, Schmidt number; SST, Sea surface temperature; TA, Total alkalinity; U, Wind speed.

which could weaken the oceanic biophysical CO_2 pumps. More than 30% of the total anthropogenic CO_2 emissions are linked to electricity generation from fossil fuels (IEA, 2019). According to the US Energy Information Administration (EIA), fossil-fuel-based electricity generation increased from 5,589 TWh to 16,833 TWh between 1980 and 2021 (https://www.eia.gov/international/overview/world; lastly accessed on 2 January 2024).

The global air–sea CO_2 flux has been estimated using large datasets of surface CO_2 partial pressure (pCO_2) for open and coastal oceans (Landschützer et al., 2016; Laruelle et al., 2017). This flux varies over time and space depending on hydrographic conditions, biological processes, and air–sea interactions. Sea surface temperature (SST) is particularly critical in calculating the air–sea CO_2 flux from surface pCO_2 observations. It is generally established that thermal and non-thermal upper-ocean factors can be used to identify seasonal fluctuations in the surface pCO_2, based on the thermodynamic relationship between seawater pCO_2 and temperature (e.g., 4.23% °C^{-1}; Takahashi et al., 1993; Takahashi et al., 2002). This relationship includes the impact of temperature on the solubility of CO_2 and the dissociation constants of carbonic acid in seawater. The air–sea CO_2 fluxes largely depend on CO_2 gas solubility (related to SST), the gas transfer velocity (related to wind speed), and the relative difference between the atmospheric and seawater pCO_2. Moreover, both in open and coastal oceans, a general latitudinal trend, with carbon sinks in high latitudes and carbon sources in the tropics, highlights the effect of the SST on pCO_2 (Roobaert et al., 2019).

In coastal oceans, pCO_2 variability remains highly uncertain due to the data sparsity and the complexity of physical and biogeochemical processes, including riverine discharge of carbon and nutrients (Chen & Borges, 2009; Cai et al., 2020; Upadhyay et al., 2023). Another concern is the discharge of anthropogenic thermal energy into water bodies via the cooling water used to remove excess heat from coal, gas, oil, and nuclear power plants. Indeed, the availability of cooling water is an essential factor in site selection for thermal plants, meaning that 55.5% and 33.4% of the thermal power plants worldwide are located within 5 km of large rivers and 20 km of coastlines, respectively (Lohrmann et al., 2019). The regional impact of the discharge of heated water in the form of a dramatic increase in the SST has been reported at different locations in coastal oceans (Madden et al., 2013; Huang et al., 2019; Lin et al., 2021). This thermal effect reduces the ocean's ability to absorb atmospheric CO_2 due to an increase in positive ΔpCO_2 (i.e., seawater pCO_2 minus atmospheric pCO_2) in source regions and a decrease in negative ΔpCO_2 in sink regions. However, the increase in pCO_2 due to cooling water discharge (CWD) from power plants has not yet been systematically documented in coastal oceans. This additional perturbation of pCO_2 with local biological and physical activity may lead to greater regional variation in surface carbonate parameters and the CO_2 flux in estuaries and coastal oceans. Furthermore, an increasing number of thermal power plants are being built in coastal areas due to the vulnerability of freshwater sources such as rivers and lakes to drought and extreme heat (van Vliet et al., 2016). Consequently, these regions represent a significant source of uncertainty in regional estimates of the air–sea CO_2 flux due to high spatiotemporal pCO_2 variability.

In the present study, we investigated the effect of CWD on the air–sea CO_2 flux using data from power plants worldwide. Initially, we first estimated the water use intensity (km^3 TWh^{-1}) for power plants based on the relationship between the CWD and electricity generation using a local dataset from South Korea since key information, such as the cooling water temperature, is not widely available. The amount of CWD in coastal areas globally was then calculated based on the total electricity generation and our estimate of the water use intensity. We then compared our estimates of the water use intensity and CWD with those calculated in past studies from various estimates and datasets. Following this, we approximated the impact of the CWD on the decrease in the atmospheric CO_2 uptake of coastal oceans, which varies depending on the background air–sea CO_2 gradients, wind speeds, and mixed layer depth. We used global datasets for seawater total dissolved inorganic carbon (DIC) and total alkalinity (TA) to evaluate global and regional thermal-driven changes in pCO_2 and DIC and compared them with regional carbon fluxes in coastal areas.

2 Materials and methods

We extracted data for various power plant variables, including fuel type, capacity, and electricity generation, from the Global Power Plant Database V1.3.0 (https://datasets.wri.org/dataset/globalpowerplantdatabase; last updated in June 2021). The database covers about 35,000 coal, gas, oil, and nuclear power plants from 167 countries and includes the geolocation of each power plant for 2017. The annual electricity generation for coastal areas was calculated for power plants within ~20 km of the coastline. It is posited that power plants within this range utilize seawater for cooling purposes (Lohrmann et al., 2019). We assumed that these coastal power plants employ a once-through cooling system drawing water from a large water body such as the ocean or a river.

We estimated the amount of cooling water reaching the coastal ocean by multiplying the electricity generation by the water use intensity (e.g., km^3 TWh^{-1}) derived from monthly data from South Korea. South Korea ranked as the ninth-largest energy consumer globally in 2019 (Looney, 2020) and produced 512 TWh of electricity in coastal areas, constituting ~7% of global coastal electricity generation in 2017. The electricity generation in South Korea comprised ~69% from fossil fuel sources and around ~25% from nuclear power sources (EIA's Country Analysis Brief: South Korea; available at https://www.eia.gov/international/analysis/country/KOR; lastly accessed on 2 January 2024). Monthly data for once-through cooling systems, including the electricity generation, CWD, inlet temperature, and outflow temperature, are taken from Korea Electric Power Company and Korea Hydro & Nuclear Power (KHNP). The data for nuclear power plants is restricted to research purposes and obtained from KHNP, whereas the majority of data for fossil fuel plants is publicly accessible at https://www.data.go.kr/ (lastly accessed on 2 January 2024). These data were compiled from 22 coal, gas, and oil power plants and 5 nuclear power plants, collectively accounting for ~59% of the total electricity generation between 2018 and 2020. These power plants are located in coastal areas and use seawater as a source of cooling water.

The coastal ocean data for 2017, including temperature, salinity, DIC, TA, and pCO_2, were obtained from a global 1°×1° gridded product (OceanSODA-ETHZ; Gregor & Gruber, 2021). Following Laruelle et al. (2017), our study area was defined as coastal regions within 300 km from coastlines or a depth of 1000 m (Figure 1). Daily air–sea CO_2 flux (FCO_2) was estimated using the procedure described by Wanninkhof (2014). The equation of $FCO_2 = k \times \alpha \times \Delta pCO_2$ was used, where k is the CO_2 gas transfer velocity, α is the CO_2 solubility in seawater (Weiss, 1974), and ΔpCO_2 is the air–sea pCO_2 difference (seawater pCO_2 – atmospheric pCO_2). k was defined as $k = 0.251 \times (Sc/660)^{-1/2} \times U^2$, where Sc is the Schmidt number and U is wind speed (m s^{-1}) (Wanninkhof, 2014). Wind speed data (at 10 m) was obtained from the National Centers for Environmental Prediction-Department of Energy (NCEP-DOE) Reanalysis 2 (Kanamitsu et al., 2002).

The deficits in the DIC resulting from degassing via air–sea CO_2 gas exchange depends on the Revelle factor (Revelle & Suess, 1957), which represents the fractional change in surface seawater CO_2 ($\Delta pCO_2/pCO_2$) over the fractional change in the DIC (ΔDIC/DIC). The Revelle factor was calculated from the DIC and TA using the carbonic acid dissociation constants defined by Millero (2010). The sensitivity of oceanic DIC to an increase in pCO_2 was assessed using the inverse of the Revelle factor, which varies regionally between oceans.

3 Results and discussion

3.1 Estimates of cooling water discharge from global coastal power plants

The total electricity generation worldwide estimated from the dataset with geolocation information was 19,163 TWh in 2017, which is 78.6% of the 24,394 TWh reported in the database provided by the EIA (https://www.eia.gov/international/overview/world; lastly accessed on 2 January 2024). This discrepancy may arise from the scarcity of geolocation data for wind and solar power plants (Byers et al., 2021). On the other hand, geolocation data for conventional thermal power plants are more widely available (~100%). The electric generation within 20 km of the coastline (6,838 TWh) accounts for 35.7% of the total electric generation. Regional electric generation differs notably between latitudinal bands (Figure 1). In particular, along the coastline, 28.1% and 37.9% of worldwide electricity generation are observed in the 20°N–30°N and 30°N–40°N latitude bands, respectively.

The water use intensity and thermal efficiency vary seasonally depending on the difference in temperature between the internal heat source and the external environment (De La Guardia et al., 2022). In South Korea, the outlet temperature exhibited seasonal variations, ranging from 0 to 15°C higher than the inlet temperature, with an average difference of 6.6°C between 2018 and 2020 (Supplementary Figure 1). To the best of our knowledge, there is no publicly available data for the temperature information, including the temperature of the source water and the difference between the inlet and outlet of the cooling water, that can be applied to global estimates. Therefore, the water use intensity was calculated based on the CWD and electricity generation using monthly data from 22 fossil fuel and 5 nuclear power plants in South Korea. An annual electricity generation of 375 TWh and a CWD of 58.5 km^3 has been reported from 2018 to 2020, from which the corresponding water use intensity was estimated to be 0.156 km^3 TWh^{-1}, which is consistent with the range reported in previous regional studies (0.136–0.207 km^3 TWh^{-1}) for once-through cooling systems in fossil fuel and nuclear power plants (Peer & Sanders, 2016; Pan et al., 2018; Lin et al., 2021; De La Guardia et al.,

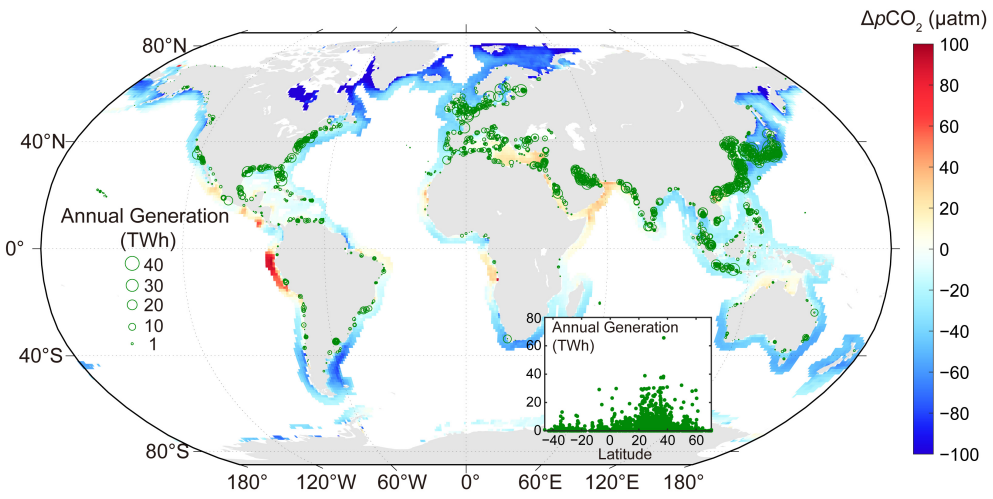

FIGURE 1
Global distribution of thermoelectric power plants and their electricity generation (green circles) within 20 km of the coastline. The color bar indicates the annual mean difference between seawater and atmospheric CO_2 partial pressure (ΔpCO_2: seawater pCO_2 – atmospheric pCO_2) of the study region. An atmospheric pCO_2 of 407 µatm is used, which is the 2017 average from flask analysis data collected at Mauna Loa, USA (19.54°N, 155.58°W) and obtained from the National Oceanic and Atmospheric Administration (NOAA)/Global Monitoring Laboratory (https://gml.noaa.gov/ccgg/; lastly accessed on 2 January 2024). The inset shows the latitudinal distribution of the annual electricity generation (TWh) of the coastal thermoelectric power plants.

2022) (Figure 2). The average water use intensity is 0.137 km^3 TWh^{-1} for fossil fuel power plants and 0.184 km^3 TWh^{-1} for nuclear power plants, which likely reflects the differences in the thermal efficiency between the two fuel sources (Figure 2). Although individual nuclear and fossil fuel plants can vary widely in their efficiency, the average thermal efficiency of fossil fuel plants (40–60%) is greater than that of nuclear plants (34–36%) (Wibisono & Shwageraus, 2016). As shown in Figure 2, coal plants in South Korea also have higher thermal efficiency and require less cooling water than nuclear power plants.

The global CWD was then calculated using annual electric generation (6,838 TWh) for coastal areas and the water use intensity estimated from the South Korea data (0.156 km^3 TWh^{-1}). Overall, 1,066 km^3 of cooling water was estimated to be discharged yearly, which is comparable to the global wastewater discharge (~1,000 km^3; Lu et al., 2018) and the discharge from Changjiang River (900 km^3; Yang et al., 2015). However, our estimate is three times higher than the reported seawater withdrawal rate (300 km^3) for coastal areas based on satellite imagery (Lohrmann et al., 2019). One reason for this difference could be that we assume that only once-through cooling systems are used in coastal areas, which can result in the overestimation of the CWD due to the higher water use intensity of once-through cooling systems compared to other cooling technologies (e.g., recirculating cooling towers and dry cooling systems). Another possible explanation is that estuaries are often found close to large rivers and oceans, which can be an important source of fresh (or brackish) water for cooling; however, our estimates did not take into account freshwater use. Despite this, it should be noted that once-though cooling systems are the most common cooling technology for the power plants built along the coastline, and differences in CWD estimates are apparent in country-level comparisons (De La Guardia et al., 2022).

To verify our methodology for estimating the CWD, our CWD estimates for China, Japan, the United States, and South Korea were compared with those from previous research. Our estimates for the CWD are 222.3, 138.7, 109.0, and 79.8 km^3 for China, Japan, the United States, and South Korea, respectively, which are higher than the 14.4, 29.4, 1.8, and 28.6 km^3 reported by Lohrmann et al. (2019). However, previously reported seawater withdrawal volumes of 108–201 km^3 for China (Zhang et al., 2016; Lin et al., 2021) are comparable to our estimates. The seawater withdrawal data reported by Zhang et al. (2016) for China in 2011 was approximately scaled for 2017 based on the annual electric generation of China between 2011 and 2017. In addition, for the

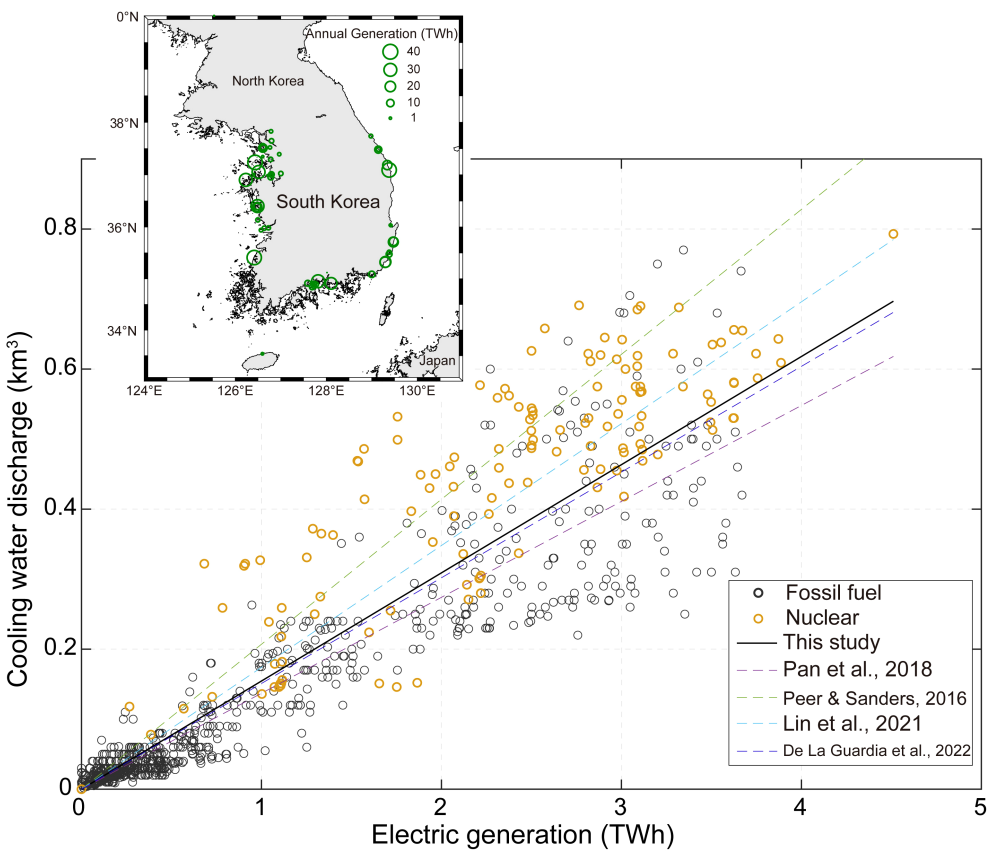

FIGURE 2
Monthly cooling water discharge (km^3) versus monthly electric generation (TWh) for 22 fossil (black circles) and 5 nuclear (yellow circles) power plants in South Korea. The water use intensity is estimated to be 0.156 km^3 TWh^{-1} (solid line), which is consistent with the range reported by previous regional studies (0.136–0.207 km^3 TWh^{-1}; dashed lines) for once-through cooling systems in fossil fuel and nuclear power plants (Peer & Sanders, 2016; Pan et al., 2018; Lin et al., 2021; De La Guardia et al., 2022). The inset shows the locations and annual electricity generation (TWh) for power plants in South Korea obtained from the Global Power Plant Database V1.3.0 (https://datasets.wri.org/dataset/globalpowerplantdatabase; lastly accessed on 2 January 2024).

United States, the reported seawater withdrawal of 31.8–42.8 km^3 (Harris & Diehl, 2019) is 29–39% of our estimates. The variation in the estimates for different countries can be attributed to the relative proportion of freshwater- and seawater-based cooling systems in coastal areas. Nevertheless, the order of magnitude difference in the estimated CWD at the country and regional level suggests that additional assessments are needed using a more extensive database for CWD based on estimates from various methods.

3.2 Change in pCO_2 and the oceanic uptake of CO_2 due to CWD

When a specific power generation capacity is given, the temperature difference (ΔT) between the inlet and outlet is inversely proportional to the amount of CWD. Therefore, this study utilized the ΔT of ~6.6°C, corresponding to the water use intensity (0.156 km^3 TWh^{-1}). This ΔT was estimated to lead to a variation of 70–170 µatm in pCO_2, which is comparable to the seasonal variation in pCO_2 observed for the temperate open ocean (<90 µatm; Takahashi et al., 2014). To examine the potential impact of the CWD on the absorption of atmospheric CO_2, we calculated the rise in the pCO_2 of the discharged water and the change in the DIC (ΔDIC) resulting from perturbations in the air–sea CO_2 flux. It should be noted that the calculation for assessing the ΔDIC was conducted using pCO_2–TA pairs, and a coefficient ($\partial \ln pCO_2/\partial SST$) of 0.0423°$C^{-1}$ (Takahashi et al., 1993; Takahashi et al., 2002) was not directly applied. This is because the influence of temperature on pCO_2 exhibited values different from 0.0423°C^{-1}, especially under low-temperature or salinity conditions (Jiang et al., 2008; Calleja et al., 2013; Gallego et al., 2018).

The upper limit of the ΔDIC was calculated assuming that the elevated pCO_2 returns to the original condition through the air–sea CO_2 exchange without considering further biophysical processes. It was also assumed that the relaxation back to initial conditions would occur independent of oceanic and meteorological variables. The meridional variation in the ΔDIC indicates that warm and salty waters in the subtropics (−57 ± 3 µmol kg^{-1}) are more sensitive to pCO_2 perturbations compared to cold polar waters with low salinity (−47 ± 6 µmol kg^{-1}; Figure 3A). For initially oversaturated seawater with respect to the atmosphere, a negative value of the ΔDIC represents the expected value from the greater release of CO_2 due to warming. Thus, a negative value for the ΔDIC for initial and post-discharge undersaturated seawater represents the probable decline in CO_2 uptake potential. Based on the expected ΔDIC and the relative contribution of CWD in each latitudinal band, we evaluated the impact of CWD on the average surface DIC (ΔDIC = −55 ± 4 µmol kg^{-1}) in global coastal waters. Overall, the estimated warming caused by CWD (1,066 km^3) could potentially lead to a reduction in the oceanic CO_2 uptake of 0.69 Tg C yr^{-1} (~2.5 Tg CO_2 yr^{-1}).

The effect of seawater pCO_2 perturbation depends on how rapidly the perturbed seawater is restored to its initial state in terms of pCO_2 and the SST. Thermal discharge to a net CO_2 source area would quickly lead to a return to the initial pCO_2 due to the enhanced sea-to-air CO_2 flux (i.e., outgassing). The thermal stratification and surface residence time associated with the seasonal SST cycle can also regulate the response of discharged water. When air–sea heat exchange (with heat loss reducing oceanic pCO_2 in accordance with $\partial \ln pCO_2/\partial SST$ = 0.027–0.0423°C^{-1}) is faster than air–sea CO_2 exchange, the pCO_2 of cooling water would recover quickly. In this case, the DIC deficit of the thermal plume would be smaller than that expected solely from CO_2 outgassing. Therefore, our estimate of ~0.69 Tg C yr^{-1} is likely to represent an upper theoretical limit based on the current data.

In addition to the upper limit estimation, we calculated ΔDIC while considering varying gas exchange rates to investigate the realistic response of discharged water associated with instantaneous warming at different wind speeds and air–sea CO_2 gradients. In the actual environment, discharged cooling water is mixed with surrounding (source) waters. Assuming a 10-fold dilution (leading to the ΔT of 0.66°C), the ΔDIC is proportionally reduced to a factor of one-tenth. Since it is challenging to observe the dilution signal with the gridded product used in this study, the assumption of one-tenth dilution was made with the expectation that ΔDIC aligns with a level comparable with accuracy and precision (± 2–3 µmol kg^{-1}) of the DIC measurement (Supplementary Figure 2). It should be noted that taking into account the dilution factor, the overall change in DIC of CWD remains relatively consistent. Initially, we calculated the ΔDIC of the source water associated with the air–sea CO_2 gas exchange using its original condition, which corresponds to an initial pCO_2 ranging from 257 to 557 µatm, and the average value of TA of 2248 µmol kg^{-1}, S = 33.7, and T = 17.1°C of the coastal ocean datasets (Supplementary Figure 2). Subsequently, we calculated the ΔDIC for the cooling water, assuming a 10-fold dilution, resulting in a temperature increase of 0.66°C. The difference in ΔDIC between source water and cooling water represents the impact of temperature elevation on air–sea CO_2 exchange and the DIC inventory.

These calculations of the realistic response of carbonate parameters associated with instantaneous warming were explicitly performed for the 6-month warming period (spring to summer) when SST increased. It was assumed that the sea-to-air heat flux was minimized during this period. Considering the average wind speed of 4 m s^{-1} between 30–40°N of our study region and an assumed mixed layer depth of 15 m, the final DIC concentration of discharged cooling water was ~27 µmol kg^{-1} lower than that of source water (Figure 4B). This decrease in DIC is primarily attributed to the enhanced CO_2 outgassing or weakened CO_2 uptake depending on the air–sea CO_2 gradient (Supplementary Figure 2C). The magnitude of the ΔDIC is ~49% of our upper limit of ~55 ± 4 µmol kg^{-1} expected from the complete relaxation of pCO_2 perturbation. Since only a 6-month period was considered, the ΔDIC was applied to half of the annual discharged water volume. Additionally, taking into account the average duration of the discharged water during the warming period, the CWD can potentially impact the surrounding water for approximately 3 months. Overall, it was estimated that the upper limit (~0.69 Tg C yr^{-1}) of the impact of CWD has reduced to ~13% of its original magnitude (~0.09 Tg C yr^{-1}).

Our estimates are sensitive to variations in wind speed, mixed layer depth, and air–sea CO_2 gradient. It is difficult to obtain precise

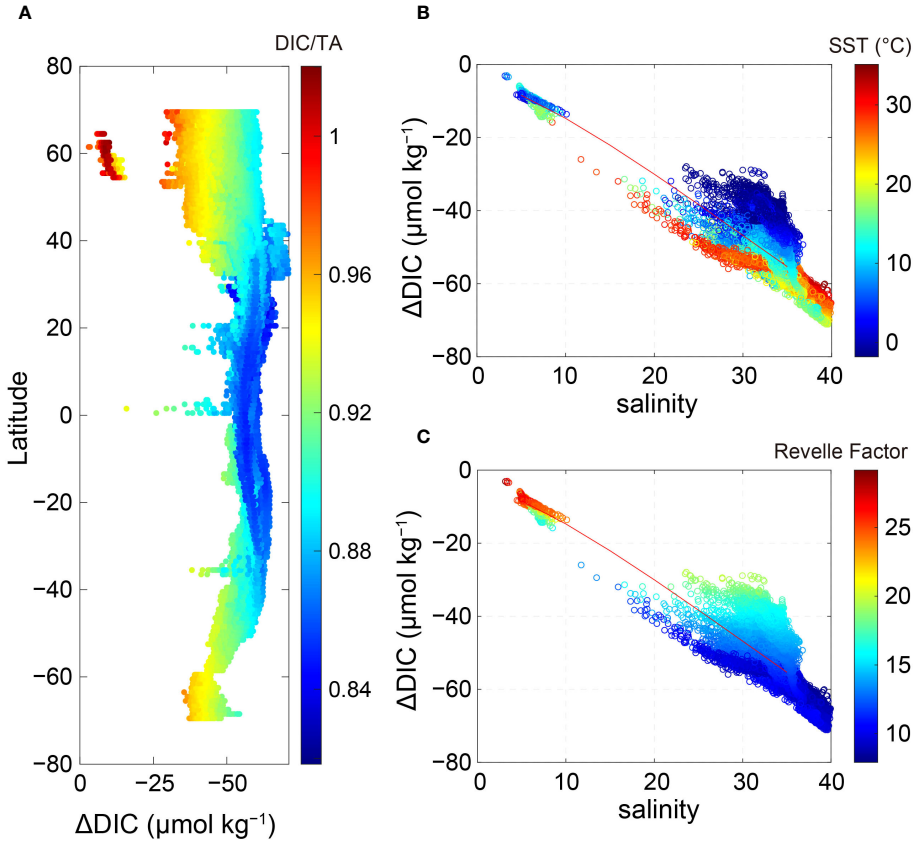

FIGURE 3
(A) Potential decrease in the total dissolved inorganic carbon (ΔDIC) of discharged cooling water. It represents the relaxation of the elevated pCO_2 to original conditions solely through air–sea CO_2 exchange, without accounting for other physical factors like mixed layer depth and warming period. Please note that the x-axis is reversed. Plots of ΔDIC and salinity are overlaid with the **(B)** SST and **(C)** Revelle factor. The red line in **(B, C)** represents the expected ΔDIC value resulting from a discharge of the assumed source water. The total alkalinity (TA) of the source water was calculated using the linear TA–salinity relationship (TA = 50.43×salinity + 548.7), which was derived from monthly TA and salinity data for coastal oceans (OceanSODA-ETHZ; Gregor & Gruber, 2021). It was assumed that the source water for cooling is initially equilibrated with atmospheric CO_2.

environmental information for individual coastal areas. Furthermore, due to the non-linear response of the ΔDIC to variations in individual factors, our exploration has been limited to simple sensitivity information within a narrow range. Deviations in wind speed by 1 m s^{-1} from the assumed 4 m s^{-1} resulted in approximately 30% change in the magnitude of ΔDIC, indicating a positive correlation (Figure 4B). Utilizing mixed layer depths of 10 and 20 m led to a 20% increase and decrease in the magnitude of ΔDIC, respectively, compared to employing a mixed layer depth of 15 m. The uncertainty associated with using gridded products to assess the biogeochemical properties of the complex coastal areas was challenging to quantify accurately. Instead, we conducted a sensitivity analysis using different air–sea CO_2 gradients (seawater pCO_2 – atmospheric pCO_2; −150 to 150 μatm). The assumed ΔpCO_2 range of ±150 μatm corresponds to 3σ (± 125 μatm) of the gridded pCO_2 database and the seasonal amplitude of pCO_2 measured at coastal areas (Torres et al., 2021). These variations of ±150 μatm contributed to an 11% difference in our ΔDIC estimate (Supplementary Figure 2C). The sensitivity of ΔDIC to variations in the pCO_2 is also significantly influenced by the Revelle factor, which will be further discussed in the following section. Due to the significant variations in ΔDIC associated with each variable, accurate quantification requires precise measurement of CO_2 and environmental parameters.

The effect of the CWD-associated carbon flux is minor compared to that of other carbon fluxes, which are several orders of magnitude higher, in the global ocean. However, for regions with significant coastal thermal pollution, this impact should be taken into account during the assessment of the regional CO_2 budget, which includes the oceanic CO_2 flux with the atmosphere and terrestrial environment (via river runoff) on a national scale. For example, China, Japan, and South Korea contribute to 43.2% of global thermoelectric generation and subsequent CWD in coastal regions. In the coastal areas of China, a CWD of ~222.3 km^3 yr^{-1} is produced by coal and nuclear power plants, which is ~25% of the discharge from Changjiang River (~900 km^3 yr^{-1}), while a CWD of 79.8 km^3 yr^{-1} estimated for South Korea is greater than the discharge from its five main rivers (~43 km^3 yr^{-1}; Lee E. et al., 2021). Of the carbon fluxes in the coastal areas of South Korea, our upper estimate for the potential decrease in the CO_2 influx (~58 Gg C yr^{-1}) is comparable to the amount of organic carbon sequestrated by a tidal flat (~71 Gg C yr^{-1}; Lee et al., 2021) and ~10% of the DIC release from the five main rivers (~450 Gg C yr^{-1}; Lee E. et al., 2021). Our estimate (~58 Gg C yr^{-1}) could decrease to ~13% when

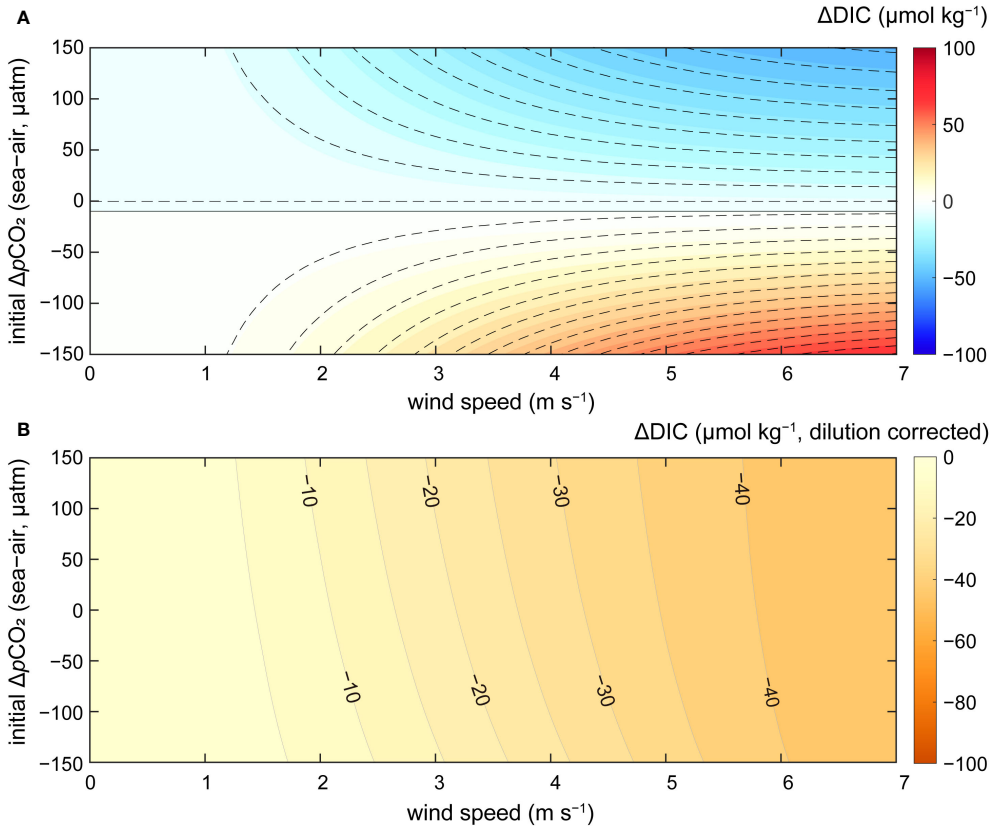

FIGURE 4
(A) The change in total dissolved inorganic carbon (ΔDIC) for both source water (dashed line) and the cooling water (indicated by color-contour) resulting from air–sea CO_2 exchange at a mixed layer depth of 15 m over 6 months. The initial condition of source water corresponds to pCO_2 values of 257–557 μatm and the average value of TA = 2248 μmol kg^{-1}, S = 33.7, and T = 17.1°C. It was assumed that the cooling water is instantaneously diluted 10-fold after being discharged, resulting in a temperature increase of 0.66°C. **(B)** The difference in DIC concentration (cooling water – source water) represents the effect of the enhanced CO_2 outgassing or weakened CO_2 uptake, which varies based on the initial pCO_2 levels. It is noted that ΔDIC in **(B)** is multiplied by a factor of 10 to account for the dilution.

considering other physical factors such as a mixed layer depth and warming period. Globally, the estimated ΔDIC due to CWD (0.09–0.69 Tg C yr^{-1}) is relatively minor (<11%) compared to the carbon sequestration rate of the top sediment (6.8 Tg C yr^{-1}; Chen & Lee, 2022) in global tidal flats (127,921 km^2).

3.3 The sensitivity of DIC to pCO_2 variation

Currently, available data for physical factors (e.g., hydrodynamics, mixed layer depth, and air–sea heat flux) are insufficient for the accurate estimation of the gas exchange timescale for the restoration of perturbed oceanic CO_2. Given the difficulty in modeling the relatively slow process of gas exchange (i.e., over weeks to months) for the CO_2, we focus on variation and heterogeneity in coastal systems with a variety of salinity and carbonate parameters. This analysis can serve as a roadmap for future attempts to measure the impact of the CWD on more specific regions (e.g., estuaries).

Buffer factors determine the relative sensitivity of carbon parameters (e.g., pCO_2, DIC, pH, and calcium carbonate saturation state) to perturbations from normal conditions. Because we assessed the potential impact of the CWD-induced change in pCO_2, the associated ΔDIC is proportional to the inverse of the conventional buffer factor (i.e., the sensitivity of pCO_2 to changes in the DIC) and varied regionally. In coastal oceans, the TA is generally higher than the DIC, with a DIC/TA ratio ranging from 0.82 to 1.02. The lowest DIC/TA ratios are observed in the warm subtropical regions with the most robust buffering capacity (Revelle factor of ~8). The lowest buffering capacity (Revelle factor of ~17) is observed in subpolar regions, where the DIC/TA ratio approaches unity (Figure 3).

Near-shore areas and estuaries are generally known as net sources of CO_2 emitted to the atmosphere due to the microbial oxidation of organic carbon and the input of poorly buffered freshwater (Chen & Borges, 2009; Cai et al., 2021). Due to the lower buffering capacities (i.e., a higher Revelle factor) in estuarine and low-salinity coastal waters, a fractional change in pCO_2 results in a weaker fractional change in the DIC compared with seawater. As the salinity approaches zero, the decrease in the DIC concentration with a lower buffer factor reduces the ΔDIC associated with CWD (Figure 3). However, when the riverine TA is high (> 1,800 μmol kg^{-1}) with a strong buffering capacity even within a lower salinity range (e.g., the Mississippi River and

Changjiang River; Cai et al., 2021), ΔDIC may exceed than expected value from the ΔDIC/salinity trend derived from the endmember (TA = ~548 μmol kg^{-1} at zero salinity) obtained from coastal ocean dataset (OceanSODA-ETHZ; Gregor & Gruber, 2021). Additionally, the ΔDIC/salinity trend can be significantly disrupted when freshwater mixes with seawater due to changes in biological production. Enhanced biological production, for example, can lead to an increase in buffer capacity. Consequently, it is essential to assess regional variations in the sensitivity to thermal stress to comprehensively evaluate the physical effect of thermal discharge on CO_2 dynamics.

4 Conclusion

To the best of our knowledge, no previous study has attempted to estimate coastal ocean pCO_2 anomalies caused by thermal discharge on a global scale. In this study, we assessed the upper limits of the variation in the DIC content of CWD associated with the reduction of the air-to-sea CO_2 flux in coastal oceans worldwide. Globally, the potential decrease in the CO_2 uptake was estimated to be 0.09–0.69 Tg C yr^{-1} due to the warming-induced increase in oceanic pCO_2. However, these preliminary assessments are constrained by the use of coarse-gridded CO_2 datasets and the omission of air–sea heat exchange. It is crucial to accurately classify the cooling type of coastal power plants and thoroughly evaluate the discharged water volume and temperature. Additionally, a higher spatial resolution carbon database, coupled with environmental factors like wind speed and mixed layer depth affecting the air–sea interaction of discharged seawater, is required. Integrating additional information from observations and models collectively contributes to understanding the duration and magnitude of pCO_2 perturbations associated with CWD, considering their diverse characteristics in various coastal environments.

Data availability statement

Publicly available datasets were analyzed in this study. This data can be found here: https://datasets.wri.org/dataset/globalpowerplantdatabase https://psl.noaa.gov/data/gridded/data.ncep.reanalysis2.html https://essd.copernicus.org/articles/13/777/2021/.

Author contributions

YK: Conceptualization, Data curation, Writing – original draft, Methodology. TK: Conceptualization, Supervision, Writing – review & editing.

Funding

The author(s) declare financial support was received for the research, authorship, and/or publication of this article. This work was supported by a National Research Foundation of Korea (NRF) grant funded by the Korean government (2021R1C1C2009977 and 2019R1A2C2089994).

Conflict of interest

The authors declare that the research was conducted in the absence of any commercial or financial relationships that could be construed as a potential conflict of interest.

Publisher's note

Supplementary material

The Supplementary Material for this article can be found online at: https://www.frontiersin.org/articles/10.3389/fmars.2024.1338832/full#supplementary-material

References

Byers, L., Friedrich, J., Hennig, R., Kressig, A., Li, X., McCormick, C., et al. (2021). A global database of power plants. *World Resour. Institute*. Available at: https://www.wri.org/research/global-database-power-plants.

Cai, W.-J., Feely, R. A., Testa, J. M., Li, M., Evans, W., Alin, S. R., et al. (2021). Natural and anthropogenic drivers of acidification in large estuaries. *Annu. Rev. Mar. Sci.* 13 (1), 23–55. doi: 10.1146/annurev-marine-010419-011004

Cai, W.-J., Xu, Y.-Y., Feely, R. A., Wanninkhof, R., Jönsson, B., Alin, S. R., et al. (2020). Controls on surface water carbonate chemistry along North American ocean margins. *Nat. Commun.* 11 (1), 2691. doi: 10.1038/s41467-020-16530-z

Calleja, M. L., Duarte, C. M., Álvarez, M., Vaquer-Sunyer, R., Agustí, S., and Herndl, G. J. (2013). Prevalence of strong vertical CO2 and O2 variability in the top meters of the ocean. *Global Biogeochem. Cycles* 27 (3), 941–949. doi: 10.1002/gbc.20081

Chen, C.-T. A., and Borges, A. V. (2009). Reconciling opposing views on carbon cycling in the coastal ocean: Continental shelves as sinks and near-shore ecosystems as sources of atmospheric CO_2. *Deep Sea Res. Part II: Topical Stud. Oceanogr.* 56 (8), 578–590. doi: 10.1016/j.dsr2.2009.01.001

Chen, Z. L., and Lee, S. Y. (2022). Tidal flats as a significant carbon reservoir in global coastal ecosystems. *Front. Mar. Sci.* 9. doi: 10.3389/fmars.2022.900896

De La Guardia, L., Zhang, Z., and Bai, X. (2022). Regional and temporal variability in water use intensity for thermoelectric power plants in the contiguous United States. *J. Clean. Prod.* 378, 134604. doi: 10.1016/j.jclepro.2022.134604

Friedlingstein, P., O'Sullivan, M., Jones, M. W., Andrew, R. M., Gregor, L., Hauck, J., et al. (2022). Global carbon budget 2022. *Earth System Sci. Data* 14 (11), 4811–4900. doi: 10.5194/essd-14-4811-2022

Gallego, M. A., Timmermann, A., Friedrich, T., and Zeebe, R. E. (2018). Drivers of future seasonal cycle changes in oceanic pCO_2. *Biogeosciences* 15 (17), 5315–5327. doi: 10.5194/bg-15-5315-2018

Gregor, L., and Gruber, N. (2021). OceanSODA-ETHZ: A global gridded data set of the surface ocean carbonate system for seasonal to decadal studies of ocean acidification. *Earth System Sci. Data* 13 (2), 777–808. doi: 10.5194/essd-13-777-2021

Harris, M. A., and Diehl, T. H. (2019). *Withdrawal and consumption of water by thermoelectric power plants in the United States, 2015* (Reston, VA: US Geological Survey), No. 2019–5103.

Hoegh-Guldberg, O., Jacob, D., Taylor, M., Guillén Bolaños, T., Bindi, M., Brown, S., et al. (2019). The human imperative of stabilizing global climate change at 1.5°C. *Science* 365 (6459), eaaw6974. doi: 10.1126/science.aaw6974

Huang, F., Lin, J., and Zheng, B. (2019). Effects of thermal discharge from coastal nuclear power plants and thermal power plants on the thermocline characteristics in sea areas with different tidal dynamics. *Water* 11 (12), 2577. doi: 10.3390/w11122577

IEA (2019). *Global Energy & CO2 Status Report* Vol. 2019 (Paris: IEA). Available at: https://www.iea.org/reports/global-energy-co2-status-report-2019/.

Jiang, L.-Q., Cai, W.-J., and Wang, Y. (2008). A comparative study of carbon dioxide degassing in river- and marine-dominated estuaries. *Limnol. Oceanogr.* 53 (6), 2603–2615. doi: 10.4319/lo.2008.53.6.2603

Kanamitsu, M., Ebisuzaki, W., Woollen, J., Yang, S.-K., Hnilo, J. J., Fiorino, M., et al. (2002). NCEP–DOE AMIP-II reanalysis (R-2). *Bull. Am. Meteorol. Soc.* 83 (11), 1631–1644. doi: 10.1175/BAMS-83-11-1631

Landschützer, P., Gruber, N., and Bakker, D. C. E. (2016). Decadal variations and trends of the global ocean carbon sink. *Global Biogeochem. Cycles* 30 (10), 1396–1417. doi: 10.1002/2015GB005359

Laruelle, G. G., Landschützer, P., Gruber, N., Tison, J. L., Delille, B., and Regnier, P. (2017). Global high-resolution monthly pCO_2 climatology for the coastal ocean derived from neural network interpolation. *Biogeosciences* 14 (19), 4545–4561. doi: 10.5194/bg-14-4545-2017

Lee, J., Kim, B., Noh, J., Lee, C., Kwon, I., Kwon, B.-O., et al. (2021). The first national scale evaluation of organic carbon stocks and sequestration rates of coastal sediments along the West Sea, South Sea, and East Sea of South Korea. *Sci. Total Environ.* 793, 148568. doi: 10.1016/j.scitotenv.2021.148568

Lee, E.-J., Shin, Y., Yoo, G.-Y., Ko, E.-B., Butman, D., Raymond, P. A., et al. (2021). Loads and ages of carbon from the five largest rivers in South Korea under Asian monsoon climates. *J. Hydrol.* 599, 126363. doi: 10.1016/j.jhydrol.2021.126363

Lin, J., Zou, X., Huang, F., and Yao, Y. (2021). Quantitative estimation of sea surface temperature increases resulting from the thermal discharge of coastal power plants in China. *Mar. pollut. Bull.* 164, 112020. doi: 10.1016/j.marpolbul.2021.112020

Lohrmann, A., Farfan, J., Caldera, U., Lohrmann, C., and Breyer, C. (2019). Global scenarios for significant water use reduction in thermal power plants based on cooling water demand estimation using satellite imagery. *Nat. Energy* 4 (12), 1040–1048. doi: 10.1038/s41560-019-0501-4

Looney, B. (2020). *Statistical review of world energy* Vol. 69 (London, UK: BP Statistics). Available at: https://www.bp.com.

Lu, L., Guest, J. S., Peters, C. A., Zhu, X., Rau, G. H., and Ren, Z. J. (2018). Wastewater treatment for carbon capture and utilization. *Nat. Sustain.* 1 (12), 750–758. doi: 10.1038/s41893-018-0187-9

Madden, N., Lewis, A., and Davis, M. (2013). Thermal effluent from the power sector: an analysis of once-through cooling system impacts on surface water temperature. *Environ. Res. Lett.* 8 (3), 35006. doi: 10.1088/1748-9326/8/3/035006

Millero, F. J. (2010). Carbonate constants for estuarine waters. *Mar. Freshw. Res.* 61 (2), 139–142. doi: 10.1071/MF09254

Pan, S.-Y., Snyder, S. W., Packman, A. I., Lin, Y. J., and Chiang, P.-C. (2018). Cooling water use in thermoelectric power generation and its associated challenges for addressing water-energy nexus. *Water-Energy Nexus* 1 (1), 26–41. doi: 10.1016/j.wen.2018.04.002

Peer, R. A., and Sanders, K. T. (2016). Characterizing cooling water source and usage patterns across US thermoelectric power plants: a comprehensive assessment of self-reported cooling water data. *Environ. Res. Lett.* 11 (12), 124030. doi: 10.1088/1748-9326/aa51d8

Revelle, R., and Suess, H. E. (1957). Carbon dioxide exchange between atmosphere and ocean and the question of an increase of atmospheric CO_2 during the past decades. *Tellus* 9 (1), 18–27. doi: 10.1111/j.2153-3490.1957.tb01849.x

Roobaert, A., Laruelle, G. G., Landschützer, P., Gruber, N., Chou, L., and Regnier, P. (2019). The spatiotemporal dynamics of the sources and sinks of CO_2 in the global coastal ocean. *Global Biogeochem. Cycles* 33 (12), 1693–1714. doi: 10.1029/2019GB006239

Takahashi, T., Olafsson, J., Goddard, J. G., Chipman, D. W., and Sutherland, S. C. (1993). Seasonal variation of CO_2 and nutrients in the high-latitude surface oceans: A comparative study. *Global Biogeochem. Cycles* 7 (4), 843–878. doi: 10.1029/93GB02263

Takahashi, T., Sutherland, S. C., Chipman, D. W., Goddard, J. G., Ho, C., Newberger, T., et al. (2014). Climatological distributions of pH, pCO_2, total CO_2, alkalinity, and $CaCO_3$ saturation in the global surface ocean, and temporal changes at selected locations. *Mar. Chem.* 164, 95–125. doi: 10.1016/j.marchem.2014.06.004

Takahashi, T., Sutherland, S. C., Sweeney, C., Poisson, A., Metzl, N., Tilbrook, B., et al. (2002). Global sea–air CO_2 flux based on climatological surface ocean pCO_2, and seasonal biological and temperature effects. *Deep Sea Res. Part II: Topical Stud. Oceanogr.* 49 (9), 1601–1622. doi: 10.1016/S0967-0645(02)00003-6

Torres, O., Kwiatkowski, L., Sutton, A. J., Dorey, N., and Orr, J. C. (2021). Characterizing mean and extreme diurnal variability of ocean CO2 system variables across marine environments. *Geophys. Res. Lett.* 48 (5), e2020GL090228. doi: 10.1029/2020GL090228

Upadhyay, P., Prajapati, S. K., and Kumar, A. (2023). Impacts of riverine pollution on greenhouse gas emissions: A comprehensive review. *Ecol. Indic.* 154, 110649. doi: 10.1016/j.ecolind.2023.110649

van Vliet, M. T. H., Wiberg, D., Leduc, S., and Riahi, K. (2016). Power-generation system vulnerability and adaptation to changes in climate and water resources. *Nat. Climate Change* 6 (4), 375–380. doi: 10.1038/nclimate2903

Wanninkhof, R. (2014). Relationship between wind speed and gas exchange over the ocean revisited. *Limnol. Oceanogr.: Methods* 12 (6), 351–362. doi: 10.4319/lom.2014.12.351

Weiss, R. F. (1974). Carbon dioxide in water and seawater: the solubility of a non-ideal gas. *Mar. Chem.* 2 (3), 203–215. doi: 10.1016/0304-4203(74)90015-2

Wibisono, A. F., and Shwageraus, E. (2016). Thermodynamic performance of pressurized water reactor power conversion cycle combined with fossil-fuel superheater. *Energy* 117, 190–197. doi: 10.1016/j.energy.2016.10.060

Yang, S. L., Xu, K. H., Milliman, J. D., Yang, H. F., and Wu, C. S. (2015). Decline of Yangtze River water and sediment discharge: Impact from natural and anthropogenic changes. *Sci. Rep.* 5 (1), 12581. doi: 10.1038/srep12581

Zhang, C., Zhong, L., Fu, X., Wang, J., and Wu, Z. (2016). Revealing water stress by the thermal power industry in China based on a high spatial resolution water withdrawal and consumption inventory. *Environ. Sci. Technol.* 50 (4), 1642–1652. doi: 10.1021/acs.est.5b05374